KMT9 controls stemness and growth of colorectal cancer

Christopher Berlin[1,9,10], Félicie Cottard[2,10], Dominica Willmann[2], Sylvia Urban[2], Stephan M. Tirier[3,4], Lisa Marx[1], Karsten Rippe[3,4], Mark Schmitt[5], Valentina Petrocelli[5], Florian R. Greten[5,6,7], Stefan Fichtner-Feigl[1], Rebecca Kesselring[1], Eric Metzger[2,8] and Roland Schüle[2,8]

[1]Klinik für Allgemein- und Viszeralchirurgie, Klinikum der Albert-Ludwigs-Universität Freiburg, Germany.
[2]Klinik für Urologie und Zentrale Klinische Forschung, Klinikum der Albert-Ludwigs-Universität Freiburg, Germany.
[3]German Cancer Research Center (DKFZ) & Bioquant, Division of Chromatin Networks, Heidelberg, Germany.
[4]Deutsches Konsortium für Translationale Krebsforschung, Heidelberg, Germany.
[5]Institut für Tumorbiologie und experimentelle Therapie, Georg-Speyer-Haus Frankfurt/Main, Germany.
[6]Frankfurt Cancer Institute, Goethe Universität Frankfurt, Frankfurt/Main, Germany.
[7]Deutsches Konsortium für Translationale Krebsforschung, Frankfurt/Mainz Germany.
[8]Deutsches Konsortium für Translationale Krebsforschung, Freiburg, Germany.
[9]IMM-PACT Clinician Scientist Program, Medizinische Fakultät, Universität Freiburg Freiburg, Germany.
[10]These authors contributed equally to this work: Christopher Berlin, Félicie Cottard

Running title
KMT9α ablation impairs colorectal tumourigenesis

Keywords
colorectal cancer, cancer stem/initiating cells, KMT9

Corresponding author
Roland Schüle, University of Freiburg Medical Center, Department of Urology, Breisacherstrasse 66, D-79106 Freiburg, Germany, Phone: +49-761-270-63100, Fax:+49-761-270-63110, roland.schuele@uniklinik-freiburg.de

Conflict of interest disclosure statement
All authors declare no competing interests.

Other notes
Word count : 4997 words
Number of figures : 4 Figures + 4 Supplementary Figures
Tables: 3 Supplementary Tables

Abstract

Colorectal cancer (CRC) is among the leading causes of cancer-associated deaths worldwide. Treatment failure and tumor recurrence due to survival of therapy-resistant cancer stem/initiating cells represent major clinical issues to overcome. In this study, we identified lysine methyltransferase 9 (KMT9), an obligate heterodimer composed of KMT9α and KMT9β that monomethylates histone H4 at lysine 12 (H4K12me1), as an important regulator in colorectal tumorigenesis. KMT9α and KMT9β were overexpressed in CRC and colocalized with H4K12me1 at promoters of target genes involved in the regulation of proliferation. Ablation of KMT9α drastically reduced colorectal tumorigenesis in mice and prevented the growth of murine as well as human patient-derived tumor organoids. Moreover, loss of KMT9α impaired the maintenance and function of CRC stem/initiating cells and induced apoptosis specifically in this cellular compartment. Together, these data suggest that KMT9 is an important regulator of colorectal carcinogenesis, identifying KMT9 as a promising therapeutic target for the treatment of CRC.

Statement of significance

The H4K12 methyltransferase KMT9 regulates tumor cell proliferation and stemness in colorectal cancer, indicating that targeting KMT9 could be a useful approach for preventing and treating this disease.

Introduction

Colorectal cancer (CRC), which includes hereditary, sporadic, and colitis-associated forms, is one of the leading causes of cancer-associated deaths worldwide (1). Four distinct consensus molecular CRC subtypes (CMS1-4) have been defined based on gene expression signatures, DNA methylation status, somatic copy number alterations, microRNA regulation changes and presence of genetic aberrations in tumour suppressor genes (e.g. tumor protein p53 (*TP53*), adenomatous polyposis coli protein (*APC*)) or oncogenes (e.g. kristen rat sarcoma viral oncogenes (*KRAS*)) (2-6). To date, systemic therapeutic options for CRC include chemotherapy (adjuvant and neo-adjuvant) and to a lesser extent, therapeutic antibodies directed against growth factor receptors e.g. vascular endothelial growth factor receptor (VEGFR) (7). Despite treatment, 30% to 40% of human patients relapse and suffer from tumour recurrence (8). This has been attributed to the acquirement of genetic aberrations during therapy and survival of cancer stem/initiating cells (CSCs) (9). CSCs and adult intestinal stem cells in the healthy gut have similar characteristics with respect to their self-renewal and differentiation capacity (10). For example, leucine rich repeat containing g-protein-coupled receptor 5 *(LGR5)*, a well-established target of the *WNT* signalling pathway, is expressed in benign intestinal stem cells and also defined as a CSC marker since *LGR5*-expressing (*LGR5*$^{+}$) tumour cells have a high clonogenic capacity (11-13). Currently, resistant CSC populations are poorly characterized and therapeutic strategies for targeting CSCs remain to be identified (14,15). One important feature of CSCs is their dynamic ability to switch between proliferative or differentiated states by modulating gene expression, which suggests the existence of epigenetic regulation (16).

Histone methyltransferases (HMTs) catalyse the transfer of a methyl group from S-adenosyl-methionine (SAM) to lysine or arginine residues of histones. Histone methylation regulates various biological processes including proliferation, cell cycle and stemness (17). Aberrant expression of histone methytransferases contributes to

global changes of the histone methylation landscape, which has been associated with CRC development, progression and patient survival (18). Therefore, targeting epigenetic regulators such as HMTs has been proposed as therapeutic strategy for CRC (19-21).

Recently, we identified the novel histone lysine methyltransferase KMT9 (22). KMT9 functions as an obligatory heterodimer composed of KMT9α (also named N6AMT1) and KMT9β (also named TRMT112), and their interaction is required for SAM binding and methyltransferase activity (22). KMT9 monomethylates lysine 12 of histone H4 (H4K12me1), thereby controlling genes that regulate proliferation of prostate and lung cancer cells (22,23). Of note, high levels of KMT9 have been associated with poor patient survival in prostate and lung cancer (22,23). Here, we investigated the function of KMT9 in CRC in vitro in human and murine organoid systems, as well as in vivo in murine models of CRC. Our data demonstrate that KMT9 is an essential regulator of CRC cell proliferation and stemness, which establishes KMT9 as a potential therapeutic target for CRC.

Materials and methods

Plasmids

pLenti6-miKMT9α was constructed by inserting the DNA sequence corresponding to a miRNA against human KMT9α into pLenti6/V5-DEST according to the manufacturer's instructions (Life Technologies). Cloning details can be obtained upon request. Details regarding the miRNA sequences used for the cloning can be found in the Supplementary Table S1.

TCGA data analysis

Normalized TCGA gene expression data were downloaded with TCGA-Assembler Version 2.0 (https://github.com/compgenome365/TCGA-Assembler-2) (.rsem.genes.normalized_results) and CMS classification of human CRC samples was calculated using CMScaller, a package in R, as previously described (24).

Mouse studies

$Apc^{fl/fl}$ $p53^{fl/fl}$ $Kras^{G12D/+}$ $Kmt9\alpha^{fl/fl}$, $Apc^{fl/fl}$ $p53^{fl/fl}$ $Kras^{G12D/+}$ $Kmt9\alpha^{+/+}$, Rosa26-CreERT2x$Kmt9\alpha^{wt/wt}$ ($Kmt9\alpha^{wt/wt}$), Rosa26-CreERT2x$Kmt9\alpha^{fl/fl}$ ($Kmt9\alpha^{ind\text{-}fl/fl}$), Villin1 (Vil1)-CreERT2x$Kmt9\alpha^{wt/wt}$ ($Kmt9\alpha^{IEC\text{-}wt/wt}$), Villin1 (Vil1)-CreERT2 x$Kmt9\alpha^{fl/fl}$ ($Kmt9\alpha^{IEC\text{-}fl/fl}$) mice were used for organoids generation and in vivo experiments. The mice were maintained in a temperature- and humidity-controlled animal facility with a 12h light/dark cycle and free access to water. Animals were sacrificed using cervical dislocation and tissues were immediately collected for further experiments.

AOM/DSS treatment

$Kmt9\alpha^{wt/wt}$, $Kmt9\alpha^{ind\text{-}fl/fl}$, $Kmt9\alpha^{IEC\text{-}wt/wt}$ and $Kmt9\alpha^{IEC\text{-}fl/fl}$ mice between 10-12 weeks of age were given an intraperitoneal injection of 10mg/kg body weight of AOM (Sigma).

Each experiment was conducted using 24 mice from different litters [n=12 control mice ($Kmt9\alpha^{wt/wt}$/ $Kmt9\alpha^{IEC\text{-}wt/wt}$) and n=12 $Kmt9\alpha^{ind\text{-}fl/fl}$ or $Kmt9\alpha^{IEC\text{-}fl/fl}$ mice]. One week after the first intraperitoneal AOM injection, animals were given *ab libitum* access to drinking water with 1.25% DSS (MP Biomedicals) for seven days followed by another seven days of normal drinking water, for a total of 5 cycles. A second intraperitoneal AOM injection was given after the first cycle. For in vivo investigation of KMT9α, mice were injected with 1mg of tamoxifen for five days and fed with tamoxifen containing food during the entire procedure. Body weight was measured once a week. Following the last cycle of normal drinking water, mice were sacrificed using cervical dislocation. Tumours were measured with a caliper and tumour volume was calculated by the formula $V=4/3 \times 3.142 \times ((width+length)/4)^3$. Tumours were fixed in 10% formalin for subsequent embedding or alternatively frozen in liquid nitrogen for subsequent analyses.

Organoid isolation

For establishment of healthy colon organoids, colonic crypts of C57BL/6 mice were isolated as described previously (25). For generation of APKK (Apc^{KO}/$Kras^{G12D}$/$p53^{KO}$ /$Kmt9\alpha^{KO}$) and APK (Apc^{KO}/$Kras^{G12D}$/$p53^{KO}$) organoids, colonic crypt of $Apc^{fl/fl}$ $p53^{fl/fl}$ $Kras^{G12D/+}$ $Kmt9\alpha^{fl/fl}$ and $Apc^{fl/fl}$ $p53^{fl/fl}$ $Kras^{G12D/+}$ $Kmt9\alpha^{+/+}$ mice were isolated as described previously (25). The deletion of the floxed sequences was mediated by infection with Cre-expressing adenovirus (BioCat GmbH). For generation of AOM/DSS tumour organoids, colonic tumours were excised from $Kmt9\alpha^{wt/wt}$ or $Kmt9\alpha^{ind\text{-}fl/fl}$ mice after AOM/DSS treatment. Tumour tissue was manually dissected and a single cell suspension containing tumour stem cells was generated using the Tumour Dissociation Kit, mouse (Miltenyi Biotec) according to the manufacturer's protocol. Patient derived organoids (PDOs) were isolated from human CRC tissue using Tumor Dissociation Kit, human (Miltenyi Biotec) according to the manufacturer's protocol. The

single cells obtained were resuspended in a solution containing growth factor-reduced Matrigel (Corning) and Advanced DMEM-F12 medium (Thermo Fisher) in a 1:1 ratio. For each dome, approximately 1000 cells were seeded in a 50μl drop of Matrigel/Advanced DMEM-F12 in 24-well plates. The matrigel was allowed to polymerize at 37°C for 20 minutes and then covered with 600μl of culture medium.

Organoid culture

Healthy colon organoids and CRC PDOs were maintained in IntestiCult™ Organoid Growth Medium [Stemcell Technologies, catalog #06005 (for mouse organoids) and catalog #06010 (for human organoids)] supplemented with penicillin/streptomycin. Mouse tumour organoids were maintained in basal medium [Advanced DMEM-F12 supplemented with penicillin/streptomycin, HEPES 10mmol/l (Invitrogen), Glutamax 1x (Invitrogen), N2 1x (Gibco), B27 1x (Gibco), and N-Acetylcysteine 1mmol/l (Sigma)]. For AOM/DSS tumour organoids, the basal medium was supplemented with 50ng/mL EGF (Peprotech). After 3-5 passages, the organoids were frozen and cryopreserved as stocks for future experiments. In general, the organoids were used between passage numbers 7 and 15. For in vitro deletion of *Kmt9α*, AOM/DSS tumours organoids were treated with 1μM 4-hydroxytamoxifen (Tam) or EtOH (vehicle) as a control. Mouse and human organoids were subcultured in Matrigel every 5-7 days or every 14 days respectively.

Chromatin immunoprecipitation and sequencing (ChIP-seq)

ChIP experiments were performed as previously described (26). Two days after seeding, AOM/DSS tumour organoids were incubated with 1μM Tam or EtOH (vehicle) as a control. Five days after Tam incubation, organoids were dissociated into single cell suspension using TrypLE (Gibco). Cell pellets were washed twice with cold PBS, cross-linked with 1% PFA for 15min at 4°C and then rinsed twice with ice-cold PBS.

The pellets were resuspended in TSE I buffer (20mM Tris-HCL pH 8, 2mM EDTA, 150mM NaCL, 0.1% SDS and 1% Triton X-100) and sonicated for 1h at 4°C (Bioruptor, Diagenode). Immunoprecipitation was performed with GammaBind G-Sepharose beads (GE-Healthcare) and specific antibodies for anti-KMT9α (#27630, lot 20062017, Schüle Lab); anti-H4K12me1 (#27429, lot 27062017, Schüle Lab); anti-KMT9β (#28358, lot 03042018, Schüle Lab). Libraries were prepared from immunoprecipitated DNA according to standard methods. ChIP-seq libraries were sequenced using a HiSeq 2000 (Illumina) at the sequencing core facility of the MPI-IE, Freiburg. Reads were aligned to the mm10 build of the mouse genome using Bowtie 2 (RRID:SCR_016368) (27). Data were further analysed using the peak finding algorithm MACS 1.42 (28) using input as control. All peaks with FDR greater than 2.0% were excluded from further analysis. The reads were used to generate the genome-wide intensity profiles, which were visualized using the IGV genome browser (29). HOMER (RRID:SCR_010881) (30) was used to annotate peaks (annotatePeaks.pl) and to calculate overlaps between different peak files (mergePeaks). The genomic features (promoter, exon, intron, 3'UTR, and intergenic regions) were defined using Refseq (RRID:SCR_003496). Seqplots (http://seqplots.ga/) was used to visualize the signals in heat maps. Data are deposited under GSE150506.

Single-cell mRNA sequencing (scRNA-seq)

Two days after seeding, Kmt9α$^{ind\text{-}fl/fl}$ AOM/DSS tumour organoids were treated with 1μM Tam or EtOH (vehicle) as a control. Five days later, the organoids were dissociated into single cell suspensions using TrypLE for 20 min at 37°C. After dissociation, single cell suspensions were washed twice in PBS, centrifugated for 5 min at 300g and counted using a LUNA automated cell counter (Logos Biosystems). Single cell capture, reverse transcription and library preparation were carried out on the Chromium platform (10x Genomics) with the single cell 3' reagent v2 protocol

214 according to the manufacturer's recommendations using 1 x 10^4 cells as input per
215 reaction well. The two final libraries (Tam/EtOH (vehicle)) were pooled and sequenced
216 on two Illumina NovaSeq SP lanes (paired-end 26 bp + 96 bp). Raw sequencing data
217 were processed and aligned to the mouse genome (mm10) using the CellRanger
218 pipeline (10x Genomics version 3.1, SCR_017344). Data are deposited under
219 GSE150506. Previously published scRNA-seq data from 23 Korean CRC patients
220 (GSE132435) was analysed using Seurat v3 as described above (31). Details
221 regarding the analysis of scRNA-seq data can be found in the Supplementary
222 Materials and Methods.
223
224 **RNA sequencing (RNA-seq)**
225 RNA from AOM/DSS organoids treated with Tam or EtOH (vehicle), APK and APKK
226 tumour organoids, miCtrl or miKMT9α transduced-PDO organoids and normal colonic
227 epithelial cells was isolated using RNeasy Mini columns (Qiagen). Total RNA from
228 KMT9α-proficient and -deficient AOM/DSS tumours (n=5 for each group) was isolated
229 using TRizol (Invitrogen). RNA samples were sequenced by the standard Illumina
230 protocol to create raw sequence files (.fastq files) at Novogene, London. Reads were
231 aligned to the mm10 build of the mouse genome using STAR version 2.7
232 (RRID:SCR_004463) (32). The aligned reads were counted with HOMER software
233 (RRID:SCR_010881) (analyzeRepeats) and differentially expressed genes were
234 identified using EdgeR (RRID:SCR_012802) (33). RNA-seq experiments from tumour
235 organoids were performed in biological triplicates. P-values < 10^{-6} were considered as
236 statistically significant. For transcriptome analyses from whole-tumour tissue of
237 AOM/DSS tumours, the 3000 most significantly deregulated transcripts (2306 genes)
238 were used to perform GSEA analysis (RRID:SCR_003199). Data are deposited under
239 GSE150506.
240

Protein isolation and Western blot analysis

Fresh frozen human tumour and adjacent healthy colonic tissue were provided by the Ontario Tumour Bank, which is supported by the Ontario Institute for Cancer Research through funding provided by the Government of Ontario. Tissue was kept on ice and manually dissected and minced for subsequent RIPA lysis. For total protein isolation from organoids, Matrigel-cultured organoids were harvested using TrypLE to break up the domes and were washed with PBS. Organoids and human tissue were lysed in ice-cold RIPA buffer (1mM EDTA, 50mM Tris-HCl pH7.5, 0.1% SDS, 150mM NaCl, 1% NP-40, 1% Sodium deoxycholate) containing complete EDTA-free Protease Inhibitor Cocktail (Roche) for 10 min on ice. After centrifugation for 10 min at 13,000 rpm at 4°C, supernatant was collected and protein concentration was determined using Bradford assay. The list of the antibodies used for Western blot can be found in the Supplementary Materials and Methods.

Study approvals

Experimental mice were housed in the pathogen-free barrier facility of the University Medical Center Freiburg in accordance with institutional guidelines and all experiments were approved by the regional board.

Human tumour organoids were established at Georg-Speyer-403 Haus, Frankfurt, Germany from fresh human tumour tissue according to regional regulations and the experiments were approved by the regional ethics committee (Ethikkommission Universitätsklinikum Frankfurt/Main 274/18). Informed consent was obtained from all donors of tissue.

Statistics

Data are represented as mean ± standard error of the mean (SEM). Significance was calculated by two-tailed Student's t-test, by one-way ANOVA and Tukey's multiple comparisons test as indicated in the figure legends. Statistical significance was set to

P<0.05 and is represented as following: ****P<0.0001, ***P<0.001, **P<0.01, * P<0.05, ns: not significant. Sample sizes are indicated where appropriate.

Additional methods

Additional methods including virus production and organoid transduction, organoid size assessment, colonic epithelial cells isolation, core histone isolation, list of the antibodies used for Western blot analysis, cell proliferation assay, flow cytometry, quantitative RT-PCR analysis, single-cell mRNA sequencing (scRNA-seq), hematoxylin and eosin and immunohistochemical staining and TUNEL assay can be found in the Supplementary Materials and Methods.

Data Availability Statement

To ensure data availability, all RNA-seq, scRNA-seq and ChIP-seq data have been deposited at GEO under GSE150506. All data that support the findings of this study are available from the corresponding authors upon reasonable request without any restrictions.

Availability of materials

All unique materials are readily available from the authors without any restrictions.

Results

Colorectal tumourigenesis is modulated by KMT9α

To investigate whether KMT9 plays a functional role in CRC, we profiled *KMT9α* and *KMT9β* mRNA expression in healthy human colon and primary colon adenocarcinoma tissues. A large cohort from The Cancer Genome Atlas (TCGA) (34) of 256 CRC patients revealed a significant increase in both *KMT9α* and *KMT9β* mRNA in CRC tissue compared to healthy colon (Fig. 1A, B). CMS stratification revealed significant overexpression of *KMT9α* in CMS2-, CMS3-, and CMS4- but not in CMS1-tumours whereas *KMT9β* mRNA was significantly increased in all subtypes (Supplementary Fig. S1A, B, C). Moreover, Western blot analyses showed that both KMT9α and KMT9β protein levels were strongly increased in human CRC tissue compared to patient-matched healthy colon (Fig. 1C). We therefore hypothesized that KMT9 might play a functional role in colorectal tumourigenesis.

Since KMT9α is indispensable for KMT9's histone methyltransferase activity (22), we engineered mice with conditional *Kmt9α* alleles by flanking exon 2 and 3 with loxP sites (Kmt9α$^{fl/fl}$) to unravel potential functions of KMT9 in colorectal tumourigenesis. For initial experiments, Kmt9α$^{fl/fl}$ mice were crossed to the Rosa26-CreERT2 deleter strain (35) to produce Kmt9α$^{ind\text{-}fl/fl}$ mice for tamoxifen (Tam)-inducible deletion of *Kmt9α*. Crosses of mice with *Kmt9α* wildtype (wt) alleles to Rosa26-CreERT2 mice, referred to as Kmt9α$^{wt/wt}$, served as controls. We treated Kmt9α$^{ind\text{-}fl/fl}$ and Kmt9α$^{wt/wt}$ mice with azoxymethane (AOM) and dextran sodium sulfate (DSS) to induce inflammatory colorectal tumour growth (36,37) and established three-dimensional (3D) epithelial organoid cultures from AOM/DSS-associated tumours (Supplementary Fig. S1D). In the absence of Tam treatment, KMT9α and KMT9β protein levels were increased in four independent AOM/DSS tumour organoids from Kmt9α$^{wt/wt}$ (Ctrl) and Kmt9α$^{ind\text{-}fl/fl}$ (#1, #2, #3) mice compared to healthy colon organoids (Supplementary

Fig. S1E). This increase is in accordance with observations we made in human patient samples (Fig. 1A, B, C). Following Tam treatment, KMT9α protein was efficiently depleted in the three independent Kmt9α$^{ind\text{-}fl/fl}$ AOM/DSS tumour organoids compared to control Kmt9α$^{wt/wt}$ AOM/DSS tumour organoids (Fig. 1D). Importantly, upon loss of KMT9α, AOM/DSS tumour organoids displayed a shrinkage in size (Fig. 1E), and the proliferation rate was strongly decreased (Supplementary Fig. S1F).

To investigate whether KMT9α loss affects tumour formation and growth in vivo, Kmt9α$^{fl/fl}$ mice were crossed to the Villin1 (Vil1)-CreERT2 deleter strain (38), which allows Tam-inducible deletion of *Kmt9α* specifically in intestinal epithelial cells (IEC) of Kmt9α$^{IEC\text{-}fl/fl}$ mice (Fig. 1F). Tam-treated Kmt9α$^{IEC\text{-}fl/fl}$ mice were compared to Tam-treated Kmt9α$^{IEC\text{-}wt/wt}$ mice (hereafter termed Kmt9α$^{IEC\text{-}KO}$ and Kmt9α$^{IEC\text{-}WT}$, respectively). Upon AOM/DSS treatment, Kmt9α$^{IEC\text{-}WT}$ mice developed colorectal tumours as expected (36,37). Immunohistochemical and qRT-PCR analyses of the tumours observed in Kmt9α$^{IEC\text{-}WT}$ mice revealed a significant increase in KMT9α mRNA and protein levels in AOM/DSS tumours compared to adjacent healthy tissue (Fig. 1G and Supplementary Fig. S1G). In contrast to Kmt9α$^{IEC\text{-}WT}$ mice, Kmt9α$^{IEC\text{-}KO}$ animals displayed a dramatic decrease in tumour burden characterized by a reduced number of microscopic and macroscopic colon tumours per mouse as well as a significantly smaller tumour size and mass (Fig. 1H). The few small tumours found in Kmt9α$^{IEC\text{-}KO}$ mice displayed reduced *Kmt9α* expression in comparison to tumours in Kmt9α$^{IEC\text{-}WT}$ mice (Fig. 1I). Analysis of cell proliferation and apoptosis showed that KMT9α-depleted tumours had reduced levels of proliferation marker KI67 (Fig. 1J) and increased apoptotic activity (Fig. 1K). In the absence of AOM/DSS treatment, colon tissue from Kmt9α$^{IEC\text{-}KO}$ and Kmt9α$^{IEC\text{-}WT}$ mice did not show any apparent morphological differences (Supplementary Fig. S1H and S1I). Moreover, proliferation analysis of healthy colon crypts by KI67 staining did not reveal any significant differences between Kmt9α$^{IEC\text{-}WT}$ and Kmt9α$^{IEC\text{-}KO}$ mice without AOM/DSS treatment

(Supplementary Fig. S1J). More importantly, transcriptome analysis performed on purified epithelial colon cells from AOM/DSS treatment-naïve Kmt9α^{IEC-WT} and Kmt9α^{IEC-KO} mice revealed only 12 significantly differentially expressed genes in KMT9α-deficient compared to KMT9α-proficient colon, thereby emphasizing the specific role of KMT9α in colorectal tumour tissue (Supplementary Table S2). Together, these data demonstrate that inflammation-associated colorectal tumourigenesis in mice is controlled by KMT9α.

KMT9α controls expression of cell cycle genes in AOM/DSS tumours and organoids

To gain mechanistic insight into KMT9α-mediated gene regulation, we determined the transcriptomes of vehicle- and Tam-treated Kmt9α$^{ind-fl/fl}$ AOM/DSS tumour organoids by RNA-sequencing (RNA-seq). The intersection of the differentially expressed gene sets for the three Kmt9α$^{ind-fl/fl}$ tumour organoids revealed a common pool of 1,183 KMT9α-dependent genes (Fig. 2A). Gene set enrichment analyses (GSEA) for these 1,183 genes uncovered terms associated with “cell cycle” and “apoptosis” as significantly deregulated biological processes (Fig. 2B). Accordingly, we found a significant downregulation of numerous genes involved in cell cycle control in KMT9α-depleted AOM/DSS tumour organoids (Fig. 2C). qRT-PCR analysis validated reduced expression of cell cycle regulators such as aurora kinase b (*Aurkb*), e2f transcription factor 1 (*E2f1*), establishment of sister chromatid cohesion n-acetyltransferase 2 (*Esco2*), minichromosome maintenance complex component 6 (*Mcm6*), pcna clamp associated factor (*Pclaf*), proline rich 11 (*Prr11*), rad51 paralog c (*Rad51c*), replication protein a2 (*Rpa2*), and dna topoisomerase II alpha (*Top2a*) upon KMT9α loss (Supplementary Fig. S2A). To validate these findings, we analysed whether KMT9α depletion in AOM/DSS tumour organoids resulted in changes to the cell cycle phase distribution by flow cytometry. KMT9 depletion was associated with an increase in G0-

G1 cells and a reduction of the S phase population (Fig. 2D), which suggests that loss of KMT9 decreased cell proliferation. Importantly, these analyses also revealed an early apoptotic subG0 population in the KMT9α-depleted tumour organoids, which is consistent with our in vivo findings (Fig. 1K). Analysis of the representative AOM/DSS tumour organoids #3 uncovered significant upregulation of pro-apoptotic genes upon KMT9α depletion (Supplementary Fig. S2B). Upregulation of genes such as phorbol-12-myristate-13-acetate-induced protein 1 (*Pmaip1*) and transforming growth factor beta 2 (*Tgfb2*) was verified by qRT-PCR (Supplementary Fig. S2C). Further supporting the notion that KMT9α depletion promotes apoptosis of AOM/DSS tumour organoids, we detected an increase in cleaved caspase 3 levels (Supplementary Fig. S2D) and in annexin V-positive (annexin V^+) and DAPI-negative ($DAPI^-$) apoptotic cells (Supplementary Fig. S2E) upon loss of KMT9α. Since KMT9 writes the H4K12me1 histone mark, we asked whether ablation of KMT9α resulted in decreased H4K12me1 levels. Western blot analyses showed a strong decrease in H4K12me1 in KMT9α-depleted AOM/DSS tumour organoids #3 (Supplementary Fig. S2F). To investigate whether the differentially regulated cell cycle genes identified were direct KMT9 target genes, we analysed the genomic localisation of KMT9α, KMT9β, and H4K12me1 by ChIP-sequencing (ChIP-seq) in AOM/DSS tumour organoids #3. We uncovered 5,652 KMT9α, KMT9β, and H4K12me1 colocalisations (Fig. 2E) that were enriched around the transcription start site (TSS) of target genes (Fig. 2F). In total, we observed the presence of KMT9α, KMT9β, and H4K12me1 at the promoter of 3,239 genes (Fig. 2E). Intersection of these 3,239 targets with the 5,882 differentially expressed genes observed for AOM/DSS tumour organoids #3 uncovered 1,168 differentially expressed, direct KMT9 target genes (Fig. 2G). Gene set enrichment analysis of the direct KMT9 targets revealed a significant enrichment of terms related to cell cycle (Fig. 2H). For instance, direct target genes with promoter presence of KMT9α, KMT9β, and H4K12me1 included cell cycle regulators described above such as *Aurkb*, *Mcm6*,

Prr11, *Rad51c*, and *Rpa2* (Fig. 2I, 2C; Supplementary Fig. S2A). Importantly, global transcriptome analysis performed from whole colorectal tumour tissue obtained from AOM/DSS-treated Kmt9α^{IEC-WT} and Kmt9α^{IEC-KO} mice also revealed cell cycle regulation by KMT9, which is consistent with our data obtained from AOM/DSS organoids (Supplementary Fig. S2G and H). Together, our data show that KMT9 directly controls cell cycle progression with a concomitant control of apoptotic state.

KMT9α controls stemness and stem cell maintenance in AOM/DSS tumours and organoids

CSCs are essential for tumour initiation and maintenance, and thereby responsible for tumour relapse and treatment failure in CRC patients (7,39). To investigate whether KMT9α depletion would impact CSC function, we analysed the expression of intestinal stem cell markers in AOM/DSS tumours from Kmt9α^{IEC-WT} and Kmt9α^{IEC-KO} mice using a previously described Lgr5 intestinal stem cell (ISC) signature (40). GSEA revealed significant negative enrichment of the intratumoural ISC signature upon loss of KMT9α (Fig. 3A). Indeed, a total of 30 ISC-related genes were significantly downregulated in KMT9α-depleted compared to KMT9α-proficient tumours, notably *Apcdd1*, *Dach1*, and *Rhobtb3,* which are previously described regulators of stemness in colorectal cancer (41-43)(Fig. 3B). Importantly, GSEA performed on vehicle- and Tam-treated Kmt9α$^{ind-fl/fl}$ AOM/DSS tumour organoids also uncovered a negative enrichment of the Lgr5 signature with 117 stem cell-related genes significantly downregulated upon KMT9α depletion (Fig. 3C and D). To elucidate the transcriptomic underpinnings of KMT9 function in the CSC population, we performed single-cell mRNA sequencing (scRNA-seq) on Kmt9α$^{ind-fl/fl}$ AOM/DSS tumour organoids cultured in the presence of EtOH (vehicle) or Tam. Using a droplet-based microfluidics platform, we obtained 2340 KMT9α-proficient and 1303 KMT9α-deficient cells after quality filtering (Supplementary Fig. S3A-D). By performing unsupervised clustering and two-

dimensional embedding using uniform manifold approximation and projection (UMAP), we identified four tumour cell subpopulations based on the expression of established marker genes (11,40,44,45) and the differentiation states by pseudotime analysis: a "stem cell" (STEM) population (cluster 1), "cycling progenitor" (CP) population (cluster 2), a "transit-amplifying" (TA) cell population (cluster 3), and a "differentiated" (DIFF) cell population (cluster 4) (Fig. 3E and Supplementary Fig. S3E-L). Population-dependent gene expression analyses showed ubiquitous *Kmt9α* mRNA expression in all four cell populations and marked decrease in *Kmt9α* mRNA in KMT9α-deficient cells relative to KMT9α-proficient cells (Fig. 3F). Analysis of the cycle phase distribution based on the expression of cell cycle marker genes (Supplementary Fig. S3M) was in agreement with the role of KMT9α in cell cycle regulation described above (Fig. 2D). Furthermore, in accordance with the bulk RNA-seq data, we observed downregulation of essential S phase genes such as *Mcm6* and *Rpa2* by scRNA-seq upon KMT9α depletion (Supplementary Fig. S3N). Interestingly, numerous stem cell-related genes listed in the previously described Lgr5+ ISC signature (40) were downregulated upon loss of KMT9α in both precursor populations (Fig. 3G and 3H). In addition, we observed increased expression of pro-apoptotic genes in KMT9α-deficient STEM and CP populations, emphasizing the relevant role of KMT9 in tumoural stem cell maintenance (Fig. 3I and Supplementary Table S3). These data suggest that loss of KMT9α might affect the self-renewal potential and colony formation capacity of tumour stem/initiating cells. To test this hypothesis, single cells isolated from KMT9α-proficient and -deficient AOM/DSS tumour organoids were evaluated for anchorage-independent sphere formation in a secondary replating assay. Importantly, the secondary sphere formation capacity of cells derived from KMT9α-deficient organoids was blocked (Fig. 3J).

To corroborate these findings in vivo, we crossed Kmt9α$^{fl/fl}$ mice with the Lgr5-EGFP-IRES-CreERT2 deleter strain (11) for Tam-inducible selective Kmt9α ablation in

intestinal Lgr5^{+} stem cells. Tamoxifen-treated mice were challenged with AOM/DSS and Lgr5-expressing CSCs were intratumourally traced in vivo using enhanced green fluorescent protein (EGFP) reporter. In accordance with our hypothesis, we found that the percentage of viable Lgr5-EGFP-positive (Lgr5-EGFP^{+}) CSCs was markedly decreased upon Kmt9α loss in the collected tumours (Fig. 3K). All together, our data demonstrate the importance of KMT9 in maintaining the self-renewal potential and viability of tumour stem/initiating cells.

KMT9α is a potential therapeutic target for the treatment of CRC

Besides inflammation-induced colorectal tumourigenesis, sporadic CRC results from the progressive accumulation of genetic and epigenetic alterations (3,46). To investigate whether KMT9 loss also affects sporadic colorectal carcinogenesis driven by key human CRC mutations, we generated epithelial tumour organoids from Apc$^{fl/fl}$ p53$^{fl/fl}$ Kras$^{G12D/+}$ Kmt9α$^{fl/fl}$ and Apc$^{fl/fl}$ p53$^{fl/fl}$ Kras$^{G12D/+}$ Kmt9α$^{+/+}$ mice. Transduction of organoids with cre-expressing adenovirus resulted in APKK (Apc^{KO}/ p53^{KO}/Kras^{G12D}/Kmt9α^{KO}) and APK (Apc^{KO}/p53^{KO}/Kras^{G12D}/Kmt9α^{WT}) CRC organoids. In line with our results presented above, we observed a severe impairment in growth for KMT9α-deficient APKK organoids in comparison to KMT9α-proficient APK CRC organoids (Fig. 4A), suggesting a critical role for KMT9 in sporadic tumour progression. To unravel the mechanistic role of KMT9α in sporadic CRC, we performed RNA-seq in APK and APKK organoids. In line with our results obtained with AOM/DSS tumour organoids, we observed a significant downregulation of genes involved in cell cycle progression in APKK organoids (Fig. 4B). Furthermore, we identified 124 stem cell-related genes significantly downregulated by KMT9α depletion (Supplementary Fig. S4A). To corroborate our data in human colorectal tumours we established patient-derived organoid (PDO) cultures from four CRC patients (PDO #1, #2, #3, and #4) representing CMS2, CMS3, and CMS4 tumours (Fig. 4C). We did not consider CMS1

tumours due to the low expression levels of *KMT9α* in CMS1 compared to CMS2-4 tumour samples (Supplementary Fig. S1A). Human PDOs were transduced with lentivirus driving expression of either control miRNA (miCtrl) or miRNA directed against *KMT9α* (miKMT9α) and organoid growth was analysed in vitro. Importantly, *KMT9α* knockdown efficiently reduced tumour organoid size in all investigated PDOs (Fig. 4D and Supplementary Figs. S4B, S4C). Consistent with this morphological phenotype, transcriptomic analysis of the PDOs revealed a significant downregulation of genes involved in cell cycle progression (Fig. 4E), as well as downregulation of multiple genes involved in CSC function of CRC (Supplementary Fig. S4D), thus corroborating the results obtained in murine inflammation-induced and sporadic colorectal tumourigenesis. We next investigated the function of KMT9α in the epithelial compartment of primary tumour tissue from CRC patients. We analysed single cell transcriptome data from 23 Korean CRC patients (GSE132435) and stratified epithelial tumour cells in KMT9α -proficient and KMT9α-deficient cell populations (Supplementary Fig. S4E) (47). Interestingly, most of the genes involved in cell cycle progression and genes downregulated upon depletion of KMT9α in murine AOM/DSS and in sporadic murine CRC organoids, were also downregulated in human epithelial KMT9α-deficient CRC cells (Fig. 4F). Furthermore, we analysed the LGR5 ISC gene signature (40) and found numerous signature genes downregulated in epithelial KMT9α-deficient human CRC cells (Fig. 4G).

Together, these findings demonstrate a decisive role of KMT9α in mouse and human sporadic colorectal carcinogenesis and as well as in inflammation-induced tumourigenesis, thereby identifying inhibition of KMT9 as a highly promising single-target approach for the treatment of CRC.

Discussion

In this study, we used mouse models and tumour organoids derived from mice and human patients as well as human tumour tissue to uncover an essential role of KMT9, a novel H4K12me1 histone methyltransferase, in CRC. Our data show that growth of inflammation-induced tumours as well as sporadic CRC is dramatically reduced in the absence of KMT9α in vitro and in vivo. While we cannot exclude that additional KMT9 functions could potentially contribute to the observed phenotype, we demonstrate that a major consequence of KMT9 loss is the impairment of tumour growth via disrupting the regulation of genes involved in proliferation, cell cycle progression and apoptosis. So far, we cannot fully rule out the possibility that the loss of KMT9 is playing a role in the inflammatory or regenerative process after AOM/DSS treatment, which warrants further investigation. Moreover, we have also demonstrated that KMT9α ablation impairs tumour growth in CMS2-, CMS3-, and CMS4 PDOs. To date, it is well accepted that the inter-patient heterogeneity of CRC has clinical implications on therapeutic responses (48). Thus, future investigations have to examine different CRC subtypes for their responsiveness to targeting KMT9 in vivo.

Besides reduction of tumour growth, elimination of colorectal CSCs to prevent tumour recurrence and metastasis remains one of the biggest clinical challenges in treating CRC. To date, most therapeutic strategies rely on combination therapy of a CSC-targeting agent with eradication of tumour mass (49), where targeting of CSCs is hindered due to its similarity with benign, noncancerous stem cells. In this study, we showed that in addition to a major impact on inhibiting tumour growth, targeting KMT9 also downregulated numerous stem cell-related genes and impaired CSC function and maintenance. Thus, inhibition of KMT9 in CRC may be a promising therapy to target colorectal CSCs.

Currently, the use of epigenetic drugs as monotherapy for CRC have largely failed to improve patient outcomes (50,51). The main issues leading to the failure of these

528 epigenetic agents include intratumour and interpatient heterogeneity and the essential
529 function of epigenetic regulators in both malignant and benign cells. Importantly, we
530 found that without AOM/DSS insult, mice with specific KMT9α ablation in intestinal
531 epithelial cells survive without a noticeable phenotype and do not exhibit morphological
532 changes of the colon tissue. Thus, weak side effects of KMT9 targeting would be
533 assumed in the clinical context. In consequence, the development of small-molecule
534 inhibitors targeting KMT9 might be a promising therapeutic avenue for CRC treatment.

Acknowledgements

This work was supported by grants of the Deutsche Forschungsgemeinschaft - Project ID 413517907 to C.B., Project ID KE2164/2-1 - FOR2438 to R.K. and Project ID 192904750 - SFB 992 Medical Epigenetics, Project-ID 403222702 - SFB 1381, Project-ID 89986987 - SFB 850, Schu688/15-1, and of the European Research Council (ERC AdGrant 322844) to R.S.

We thank L. Walz, F. Pfefferle, M. Sum, and S. Schumacher for excellent technical assistance as well as B. Mauerer, H. Braumüller, J. Leung and H. Greschik for creative input and insightful comments throughout the project. B. Ritter was of great help concerning human tumour organoid experiments. We would like to acknowledge the Lighthouse Core Facility for their assistance with FACS analysis.

Author Contributions

R.S. and C.B. generated the original hypothesis. C.B., F.C., R.K., L.M., S.U., V.P. and M.S. performed experiments. S.M.T. and K.R. designed and conducted single cell RNA-seq experiments. D.W. and S.M.T. performed bioinformatics analyses. R.S., C.B., F.C., E.M., R.K., F.G. and S.F. provided intellectual contributions throughout the project. C.B., F.C., E.M. and R.S. took primary responsibility for writing the manuscript. All authors edited the manuscript.

References

1. Siegel RL, Miller KD, Jemal A. Cancer statistics, 2019. CA Cancer J Clin 2019;69(1):7-34.
2. Kuipers EJ, Grady WM, Lieberman D, Seufferlein T, Sung JJ, Boelens PG, et al. Colorectal cancer. Nat Rev Dis Primers 2015;1:15065.
3. Guinney J, Dienstmann R, Wang X, de Reynies A, Schlicker A, Soneson C, et al. The consensus molecular subtypes of colorectal cancer. Nat Med 2015;21(11):1350-6.
4. Dienstmann R, Vermeulen L, Guinney J, Kopetz S, Tejpar S, Tabernero J. Consensus molecular subtypes and the evolution of precision medicine in colorectal cancer. Nat Rev Cancer 2017;17(2):79-92.
5. Berg KCG, Eide PW, Eilertsen IA, Johannessen B, Bruun J, Danielsen SA, et al. Multi-omics of 34 colorectal cancer cell lines - a resource for biomedical studies. Mol Cancer 2017;16(1):116.
6. Linnekamp JF, Hooff SRV, Prasetyanti PR, Kandimalla R, Buikhuisen JY, Fessler E, et al. Consensus molecular subtypes of colorectal cancer are recapitulated in in vitro and in vivo models. Cell Death Differ 2018;25(3):616-33.
7. Ahmed M. Colon Cancer: A Clinician's Perspective in 2019. Gastroenterology Res 2020;13(1):1-10.
8. Duineveld LA, van Asselt KM, Bemelman WA, Smits AB, Tanis PJ, van Weert HC, et al. Symptomatic and Asymptomatic Colon Cancer Recurrence: A Multicenter Cohort Study. Ann Fam Med 2016;14(3):215-20.
9. Lytle NK, Barber AG, Reya T. Stem cell fate in cancer growth, progression and therapy resistance. Nat Rev Cancer 2018;18(11):669-80.
10. Morgan RG, Mortensson E, Williams AC. Targeting LGR5 in Colorectal Cancer: therapeutic gold or too plastic? Br J Cancer 2018;118(11):1410-18.
11. Barker N, van Es JH, Kuipers J, Kujala P, van den Born M, Cozijnsen M, et al. Identification of stem cells in small intestine and colon by marker gene Lgr5. Nature 2007;449(7165):1003-7.
12. Kemper K, Prasetyanti PR, De Lau W, Rodermond H, Clevers H, Medema JP. Monoclonal antibodies against Lgr5 identify human colorectal cancer stem cells. Stem Cells 2012;30(11):2378-86.
13. Hirsch D, Barker N, McNeil N, Hu Y, Camps J, McKinnon K, et al. LGR5 positivity defines stem-like cells in colorectal cancer. Carcinogenesis 2014;35(4):849-58.
14. Zeuner A, Todaro M, Stassi G, De Maria R. Colorectal cancer stem cells: from the crypt to the clinic. Cell Stem Cell 2014;15(6):692-705.
15. Medema JP. Targeting the Colorectal Cancer Stem Cell. N Engl J Med 2017;377(9):888-90.
16. Vaiopoulos AG, Athanasoula KC, Papavassiliou AG. Epigenetic modifications in colorectal cancer: Molecular insights and therapeutic challenges. Bba-Mol Basis Dis 2014;1842(7):971-80.
17. Chen Y, Ren B, Yang JS, Wang HY, Yang G, Xu RY, et al. The role of histone methylation in the development of digestive cancers: a potential direction for cancer management. Signal Transduct Tar 2020;5(1).
18. Jung G, Hernandez-Illan E, Moreira L, Balaguer F, Goel A. Epigenetics of colorectal cancer: biomarker and therapeutic potential. Nat Rev Gastro Hepat 2020;17(2):111-30.
19. Greer EL, Shi Y. Histone methylation: a dynamic mark in health, disease and inheritance. Nat Rev Genet 2012;13(5):343-57.
20. Huang T, Lin C, Zhong LL, Zhao L, Zhang G, Lu A, et al. Targeting histone methylation for colorectal cancer. Therap Adv Gastroenterol 2017;10(1):114-31.
21. Salz T, Li G, Kaye F, Zhou L, Qiu Y, Huang S. hSETD1A regulates Wnt target genes and controls tumor growth of colorectal cancer cells. Cancer Res 2014;74(3):775-86.
22. Metzger E, Wang S, Urban S, Willmann D, Schmidt A, Offermann A, et al. KMT9 monomethylates histone H4 lysine 12 and controls proliferation of prostate cancer cells. Nat Struct Mol Biol 2019;26(5):361-71.
23. Baumert HM, Metzger E, Fahrner M, George J, Thomas RK, Schilling O, et al. Depletion of histone methyltransferase KMT9 inhibits lung cancer cell proliferation by inducing non-apoptotic cell death. Cancer Cell Int 2020;20:52.
24. Eide PW, Bruun J, Lothe RA, Sveen A. CMScaller: an R package for consensus molecular subtyping of colorectal cancer pre-clinical models. Sci Rep 2017;7(1):16618.

25. Sato T, Stange DE, Ferrante M, Vries RG, Van Es JH, Van den Brink S, et al. Long-term expansion of epithelial organoids from human colon, adenoma, adenocarcinoma, and Barrett's epithelium. Gastroenterology 2011;141(5):1762-72.
26. Metzger E, Wissmann M, Yin N, Muller JM, Schneider R, Peters AH, et al. LSD1 demethylates repressive histone marks to promote androgen-receptor-dependent transcription. Nature 2005;437(7057):436-9.
27. Langmead B, Salzberg SL. Fast gapped-read alignment with Bowtie 2. Nat Methods 2012;9(4):357-9.
28. Zhang Y, Liu T, Meyer CA, Eeckhoute J, Johnson DS, Bernstein BE, et al. Model-based analysis of ChIP-Seq (MACS). Genome Biol 2008;9(9):R137.
29. Thorvaldsdottir H, Robinson JT, Mesirov JP. Integrative Genomics Viewer (IGV): high-performance genomics data visualization and exploration. Brief Bioinform 2013;14(2):178-92.
30. Heinz S, Benner C, Spann N, Bertolino E, Lin YC, Laslo P, et al. Simple combinations of lineage-determining transcription factors prime cis-regulatory elements required for macrophage and B cell identities. Mol Cell 2010;38(4):576-89.
31. Fachal L, Aschard H, Beesley J, Barnes DR, Allen J, Kar S, et al. Fine-mapping of 150 breast cancer risk regions identifies 191 likely target genes. Nat Genet 2020;52(1):56-73.
32. Dobin A, Davis CA, Schlesinger F, Drenkow J, Zaleski C, Jha S, et al. STAR: ultrafast universal RNA-seq aligner. Bioinformatics 2013;29(1):15-21.
33. Robinson SJ, Parkin IA. Differential SAGE analysis in Arabidopsis uncovers increased transcriptome complexity in response to low temperature. BMC Genomics 2008;9:434.
34. Chandrashekar DS, Bashel B, Balasubramanya SAH, Creighton CJ, Ponce-Rodriguez I, Chakravarthi B, et al. UALCAN: A Portal for Facilitating Tumor Subgroup Gene Expression and Survival Analyses. Neoplasia 2017;19(8):649-58.
35. Hameyer D, Loonstra A, Eshkind L, Schmitt S, Antunes C, Groen A, et al. Toxicity of ligand-dependent Cre recombinases and generation of a conditional Cre deleter mouse allowing mosaic recombination in peripheral tissues. Physiol Genomics 2007;31(1):32-41.
36. Parang B, Barrett CW, Williams CS. AOM/DSS Model of Colitis-Associated Cancer. Methods Mol Biol 2016;1422:297-307.
37. De Robertis M, Massi E, Poeta ML, Carotti S, Morini S, Cecchetelli L, et al. The AOM/DSS murine model for the study of colon carcinogenesis: From pathways to diagnosis and therapy studies. J Carcinog 2011;10:9.
38. el Marjou F, Janssen KP, Chang BH, Li M, Hindie V, Chan L, et al. Tissue-specific and inducible Cre-mediated recombination in the gut epithelium. Genesis 2004;39(3):186-93.
39. Nassar D, Blanpain C. Cancer Stem Cells: Basic Concepts and Therapeutic Implications. Annu Rev Pathol 2016;11:47-76.
40. Munoz J, Stange DE, Schepers AG, van de Wetering M, Koo BK, Itzkovitz S, et al. The Lgr5 intestinal stem cell signature: robust expression of proposed quiescent '+4' cell markers. EMBO J 2012;31(14):3079-91.
41. de Sousa E Melo F, Colak S, Buikhuisen J, Koster J, Cameron K, de Jong JH, et al. Methylation of cancer-stem-cell-associated Wnt target genes predicts poor prognosis in colorectal cancer patients. Cell Stem Cell 2011;9(5):476-85.
42. Fevr T, Robine S, Louvard D, Huelsken J. Wnt/beta-catenin is essential for intestinal homeostasis and maintenance of intestinal stem cells. Mol Cell Biol 2007;27(21):7551-9.
43. Hu X, Zhang L, Li Y, Ma X, Dai W, Gao X, et al. Organoid modelling identifies that DACH1 functions as a tumour promoter in colorectal cancer by modulating BMP signalling. EBioMedicine 2020;56:102800.
44. Takeda K, Mizushima T, Yokoyama Y, Hirose H, Wu X, Qian Y, et al. Sox2 is associated with cancer stem-like properties in colorectal cancer. Sci Rep 2018;8(1):17639.
45. Wiener Z, Hogstrom J, Hyvonen V, Band AM, Kallio P, Holopainen T, et al. Prox1 promotes expansion of the colorectal cancer stem cell population to fuel tumor growth and ischemia resistance. Cell Rep 2014;8(6):1943-56.
46. Fearon ER, Vogelstein B. A genetic model for colorectal tumorigenesis. Cell 1990;61(5):759-67.

47. Lee H-O, Hong Y, Etlioglu HE, Cho YB, Pomella V, Van den Bosch B, et al. Lineage-dependent gene expression programs influence the immune landscape of colorectal cancer. Nat Genet 2020;52(6):594-603.
48. Molinari C, Marisi G, Passardi A, Matteucci L, De Maio G, Ulivi P. Heterogeneity in Colorectal Cancer: A Challenge for Personalized Medicine? Int J Mol Sci 2018;19(12).
49. Kaiser J. The cancer stem cell gamble. Science 2015;347(6219):226-9.
50. Vincent A, Ouelkdite-Oumouchal A, Souidi M, Leclerc J, Neve B, Van Seuningen I. Colon cancer stemness as a reversible epigenetic state: Implications for anticancer therapies. World J Stem Cells 2019;11(11):920-36.
51. Baretti M, Azad NS. The role of epigenetic therapies in colorectal cancer. Curr Prob Cancer 2018;42(6):530-47.

682 **Figure 1. Colorectal tumourigenesis is modulated by KMT9α.** (**A**,**B**) *KMT9α* (**A**)
683 and *KMT9β* (**B**) mRNA expression in healthy human colon (n=39) and colon
684 adenocarcinoma (n=217) from CRC patients. Data were retrieved from The Cancer
685 Genome Atlas (TCGA) database. (**C**) Western blot showing the expression of KMT9α
686 and KMT9β in human CRC tumours and patient-matched healthy colon tissue. (**D**)
687 Western blot showing Tamoxifen (Tam)-dependent deletion of KMT9α in three
688 individual (#1, #2, and #3) AOM/DSS tumour organoid cultures, where control (Ctrl)
689 AOM/DSS tumour organoids showed no KMT9α loss. (**E**) Representative images of
690 $Kmt9\alpha^{wt/wt}$ and $Kmt9\alpha^{ind\text{-}fl/fl}$ AOM/DSS tumour organoids (#3) cultured in the presence
691 of vehicle or Tam for 7 days. Scale bars represent 50μm (left panel). Relative size of
692 tumour organoids cultured in the presence of vehicle or Tam (right panel). (**F**)
693 Schematic summarizing the treatment course of $Kmt9\alpha^{IEC\text{-}wt/wt}$ and $Kmt9\alpha^{IEC\text{-}fl/fl}$ mice
694 with azoxymethane (AOM) and dextran sodium sulfate (DSS) to induce inflammation-
695 associated tumours. KMT9α deletion in $Kmt9\alpha^{IEC\text{-}KO}$ mice was induced with Tam.
696 $Kmt9\alpha^{IEC\text{-}WT}$ mice treated with Tam served as controls. (**G**) KMT9α protein levels in
697 healthy murine colon (n=11) and AOM/DSS tumours (n=11) of $Kmt9\alpha^{IEC\text{-}WT}$ mice shown
698 by immunohistochemistry (left) and quantification of the data (right). (**H**)
699 Representative images showing fewer tumours (black arrowheads) in the colon of
700 $Kmt9\alpha^{IEC\text{-}KO}$ mice compared to $Kmt9\alpha^{IEC\text{-}WT}$ mice. Graphs show the incidence of
701 microscopic ($<0.5mm^3$) and macroscopic ($>0.5mm^3$) tumours (left), tumour size
702 (middle), and relative tumour mass (right) for $Kmt9\alpha^{IEC\text{-}WT}$ (n=9) and $Kmt9\alpha^{IEC\text{-}KO}$ (n=10)
703 mice. (**I**) Intratumoural expression of *Kmt9α* mRNA was analysed by qRT-PCR from
704 AOM/DSS tumours of $Kmt9\alpha^{IEC\text{-}WT}$ and $Kmt9\alpha^{IEC\text{-}KO}$ mice (n=8 tumours per group). (**J**)
705 Immunohistochemical staining of proliferation marker KI67 in $Kmt9\alpha^{IEC\text{-}WT}$ and
706 $Kmt9\alpha^{IEC\text{-}KO}$ AOM/DSS tumours (left) and quantification of the percentage of KI67-
707 positive nuclei (right panel). Scale bars represent 100μm, n=15 ($Kmt9\alpha^{IEC\text{-}WT}$) and n=7
708 ($Kmt9\alpha^{IEC\text{-}KO}$) AOM/DSS tumours. (**K**) TUNEL staining showing apoptosis in $Kmt9\alpha^{IEC\text{-}KO}$
709 AOM/DSS tumours in comparison to $Kmt9\alpha^{IEC\text{-}WT}$ control tumours (n=11 tumours
710 per group). All data represent means±SEM; ****P<0.0001, ***P<0.001, **P<0.01;
711 *P<0.05; two-tailed Student's t-test.
712

Figure 2. KMT9α controls expression of cell cycle genes in AOM/DSS tumours and organoids. (**A**) Intersection of genes differentially expressed in Kmt9α$^{ind\text{-}fl/fl}$ AOM/DSS tumour organoid cultures (#1, #2, and #3) upon KMT9α depletion induced by Tam (p-value < $1e^{-6}$). (**B**) Enriched biological processes obtained for the 1,183 common differentially expressed genes in AOM/DSS tumour organoids #1, #2, and #3. (**C**) Heat map showing the differential expression of genes involved in cell cycle regulation upon KMT9α depletion from three individual AOM/DSS tumour organoid cultures. FC: fold change. (**D**) Cell cycle distribution of the three separate Kmt9α$^{ind\text{-}fl/fl}$ AOM/DSS tumour organoid cultures in the presence of vehicle or Tam. Cell cycle phases were determined by flow cytometry using BrdU incorporation and 7-AAD staining. n=3 independent experiments. Data represent means±SEM; *P<0.05; two-tailed Student's t-test. (**E**) Heat maps of ChIP-seq read density for the 5,652 KMT9α, KMT9β, and H4K12me1 co-locations observed in AOM/DSS tumour organoids #3. (**F**) Average KMT9α, KMT9β, and H4K12me1 ChIP-seq read density profiles in AOM/DSS tumour organoids #3. (**G**) Direct KMT9 target genes (1,168) identified by comparing genes with KMT9α, KMT9β, and H4K12me1 localized at promoter regions to differentially expressed genes upon KMT9α depletion. (**H**) Enriched biological processes obtained for the direct KMT9 target genes. (**I**) ChIP-seq tracks showing the presence of KMT9α, KMT9β, and H4K12me1 at promoters of representative genes in AOM/DSS tumour organoids #3.

Figure 3. KMT9α controls stemness and stem cell maintenance in AOM/DSS tumours and organoids. (**A**) Gene set enrichment analysis (GSEA) of differentially expressed genes in AOM/DSS tumours from Kmt9α^{IEC-KO} compared to tumours from Kmt9α^{IEC-WT} mice uncovered significant negative enrichment of the Lgr5 ISC gene signature. (**B**) Heat map showing reduced expression of stem cell-related genes upon KMT9α loss in AOM/DSS tumours. (**C**) GSEA of differentially expressed genes in AOM/DSS tumour organoids #3 (vehicle vs Tam). (**D**) Heat map showing mRNA levels of stem cell-related genes significantly downregulated by KMT9α depletion in AOM/DSS tumour organoids. FC: fold change, p-value < 1e^{-6}. (**E**) UMAP plot showing the four subpopulations, stem cells (STEM, cluster 1), cycling progenitor cells (CP, cluster 2), transit-amplifying cells (TA, cluster 3) and differentiated cells (DIFF, cluster 4) identified in vehicle-treated Kmt9α$^{ind-fl/fl}$ AOM/DSS tumour organoids by scRNA-seq. (**F**) Violin plots showing *Kmt9α* levels in the four identified subpopulations of Kmt9α$^{ind-fl/fl}$ AOM/DSS tumour organoids following vehicle or Tam treatment. (**G**,**H**) Dot plot of the top 10 stem cell-related genes downregulated by KMT9α depletion in the STEM (**G**) and CP (**H**) populations of AOM/DSS tumour organoids. PE=percent expressed. AE=average expression. (**I**) Ridge plot representing the relative expression of pro-apoptotic genes in vehicle- and Tam-treated Kmt9α$^{ind-fl/fl}$ STEM and CP populations. (**J**) Representative images of the secondary organoid forming capacity of AOM/DSS tumour Kmt9α$^{wt/wt}$ (Ctrl) and Kmt9α$^{ind-fl/fl}$ (#3) organoids in the presence of vehicle or Tam (left). Scale bars represent 400μm. Relative number of secondary organoids after replating normalized to vehicle-treated organoids (right). Data represent means±SEM; ns: not significant, ***P<0.001; two-tailed unpaired t-test. (**K**) Contour plots depicting viable EGFP^{+}/Lgr5^{+} stem cells in AOM/DSS tumours from Kmt9α$^{Lgr5-WT}$ (n=4) and Kmt9α$^{Lgr5-KO}$ (n=4) mice.

Figure 4. KMT9α is a potential therapeutic target for the treatment of CRC. (**A**) Representative pictures of APK (Apc^{KO}/$p53^{KO}$/$Kras^{G12D}$/$Kmt9\alpha^{WT}$) and APKK (Apc^{KO}/$p53^{KO}$/$Kras^{G12D}$/$Kmt9\alpha^{KO}$) tumour organoids. Scale bars, 50μm (left). Normalized size of APK and APKK tumour organoids (upper right). Western blot showing the expression of KMT9α in APK and APKK tumour organoids (lower right). (**B**) Heat map showing significantly downregulated genes involved in cell cycle progression in APK compared to APKK tumour organoids. FC: fold change, p-value < $1e^{-6}$. (**C**) Patient-derived organoids (PDOs) were developed from CRC tumours of individual patients (#1, #2, #3, #4) covering CMS2-4 and transduced with lentivirus encoding either control miRNA (miCtrl) or miRNA directed against *KMT9α* (miKMT9α). (**D**) Reductions in organoid size were observed for PDOs #1-4 upon *KMT9α* depletion by miKMT9α relative to miCtrl. All data represent means±SEM; ****P<0.0001,*P<0.05; two-tailed Student's t-test. (**E**) Heat map showing significantly downregulated cell cycle genes in PDOs. FC: fold change, p-value < $1e^{-6}$. (**F,G**) Tumour epithelial cell population from a previously published single cell RNA-seq data set from a cohort of 23 Korean CRC patients stratified by *KMT9α* expression. Dot plot showing the top 25 cell cycle genes (**F**) and stem cell-related genes (**G**) downregulated in KMT9α-deficient epithelial CRC cells compared to KMT9α-proficient cells. PE=percent expressed. AE=average expression.

Figure 1

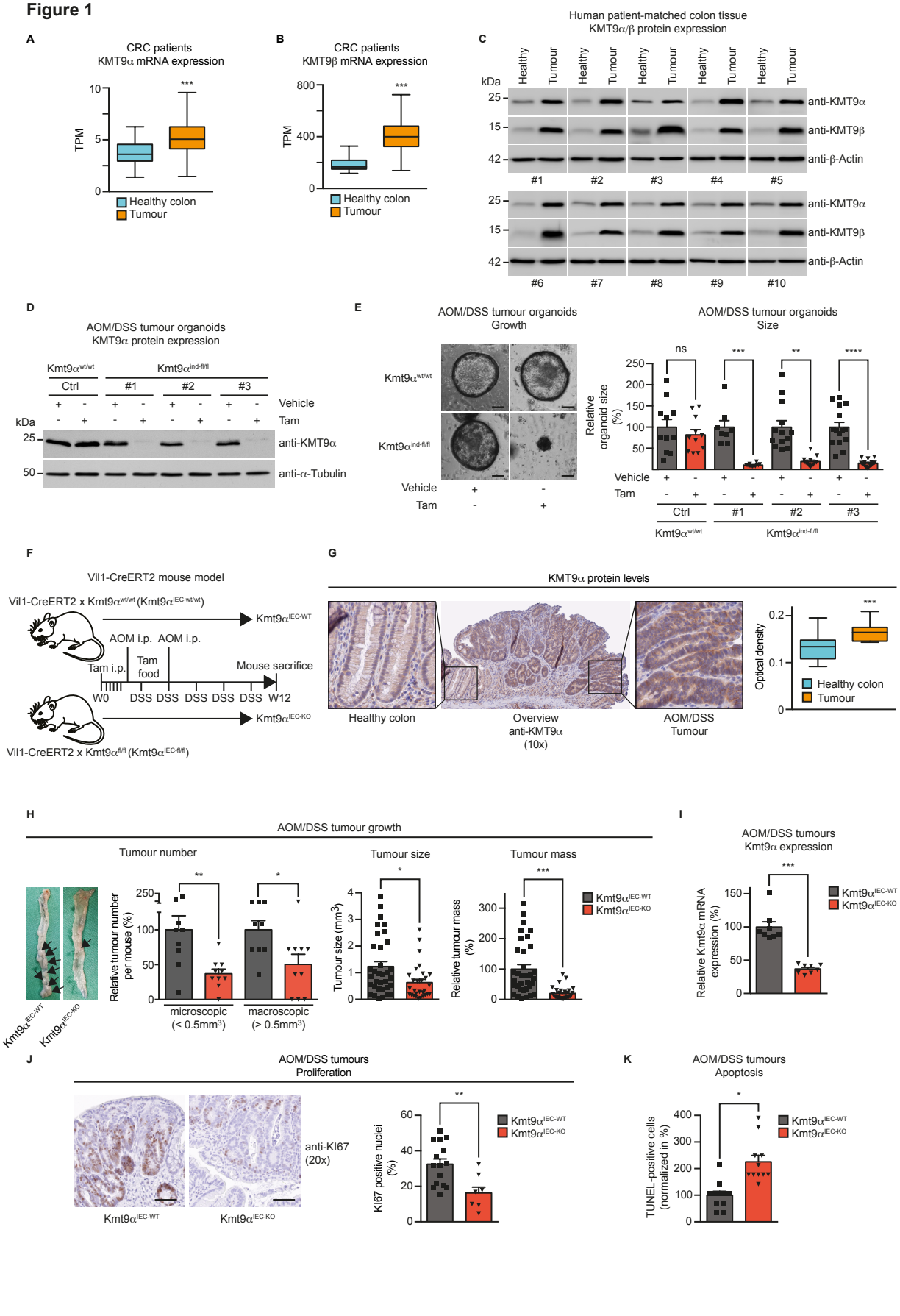

Figure 2

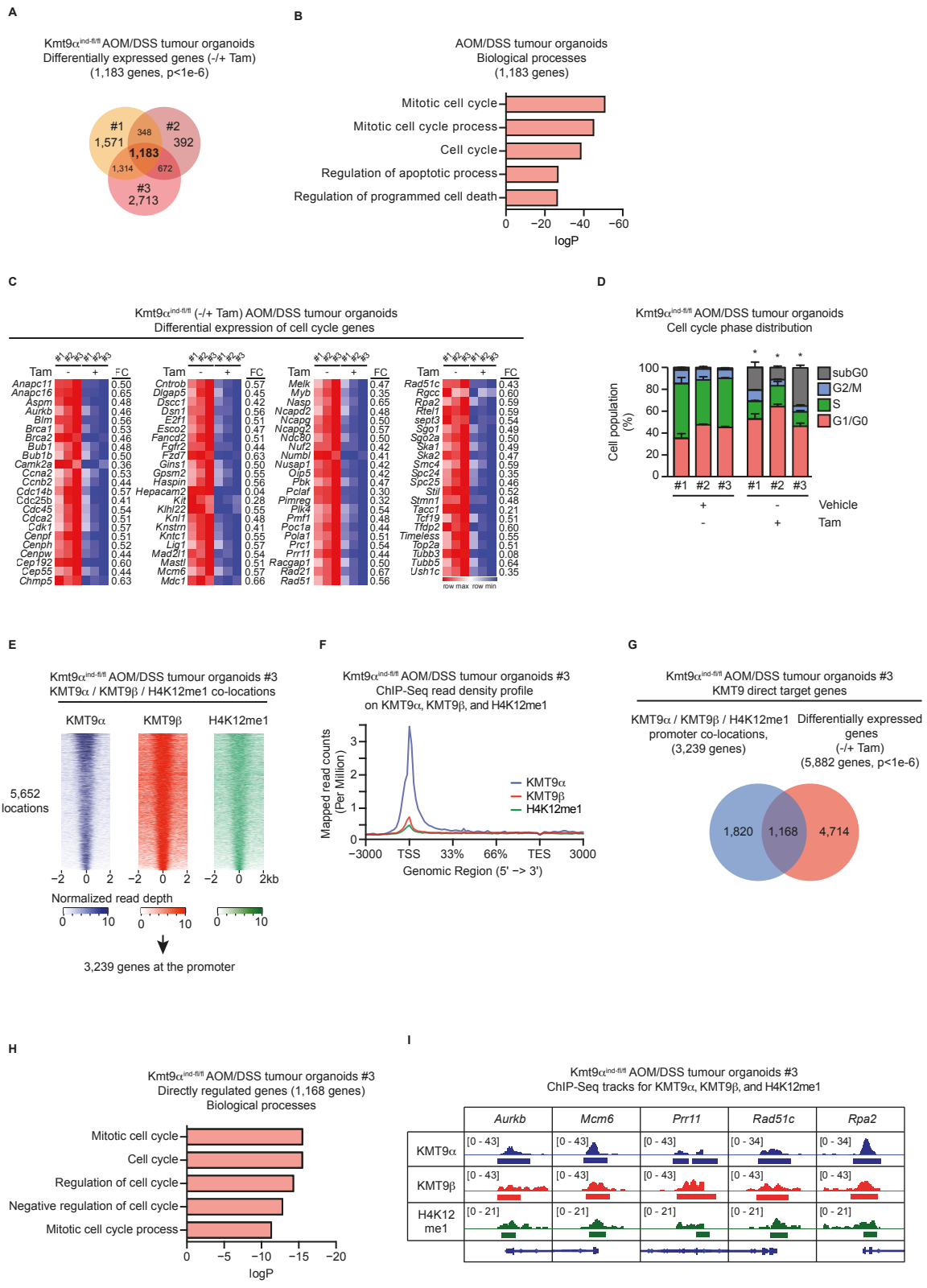

Figure 3

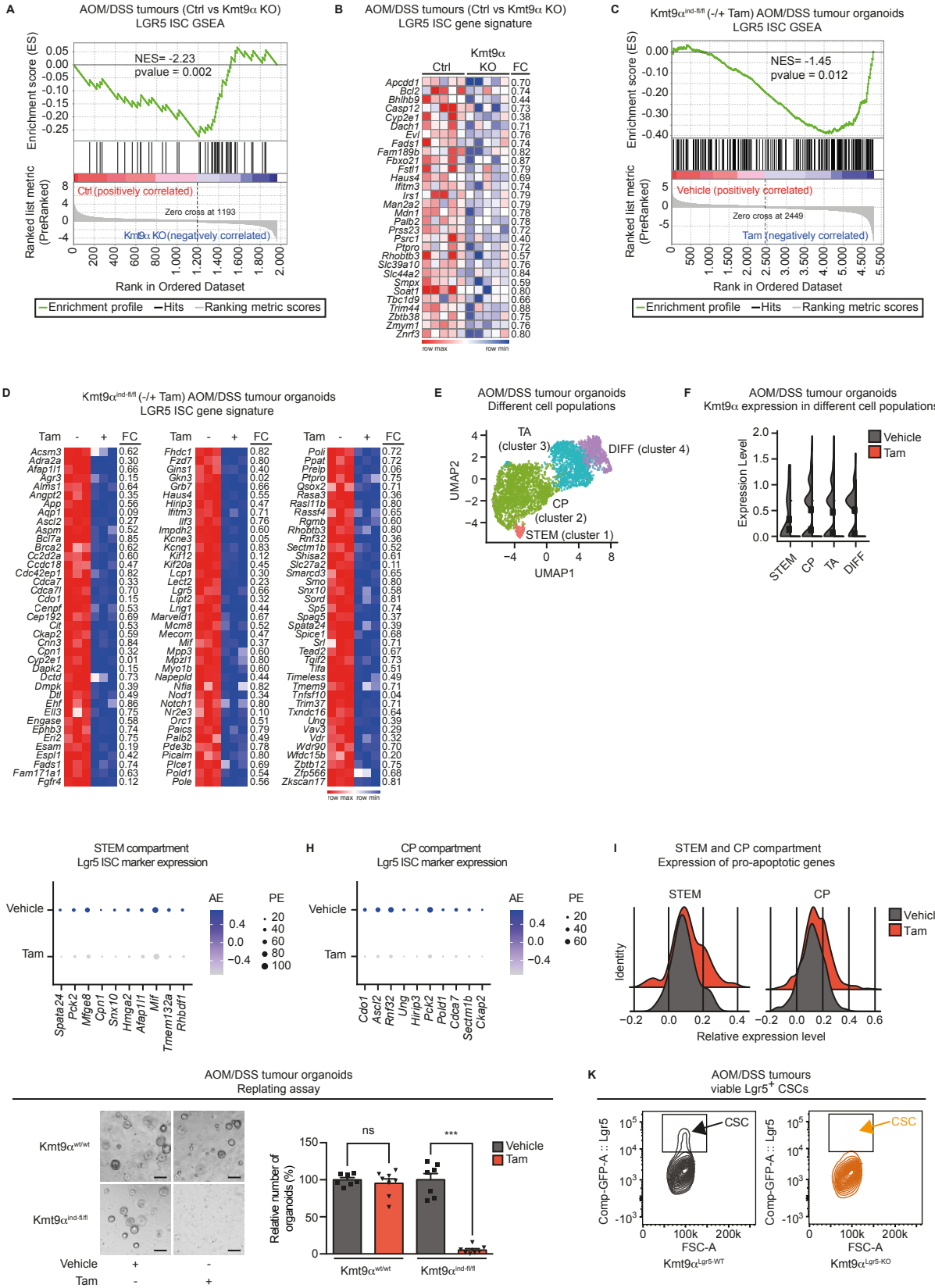

Figure 4

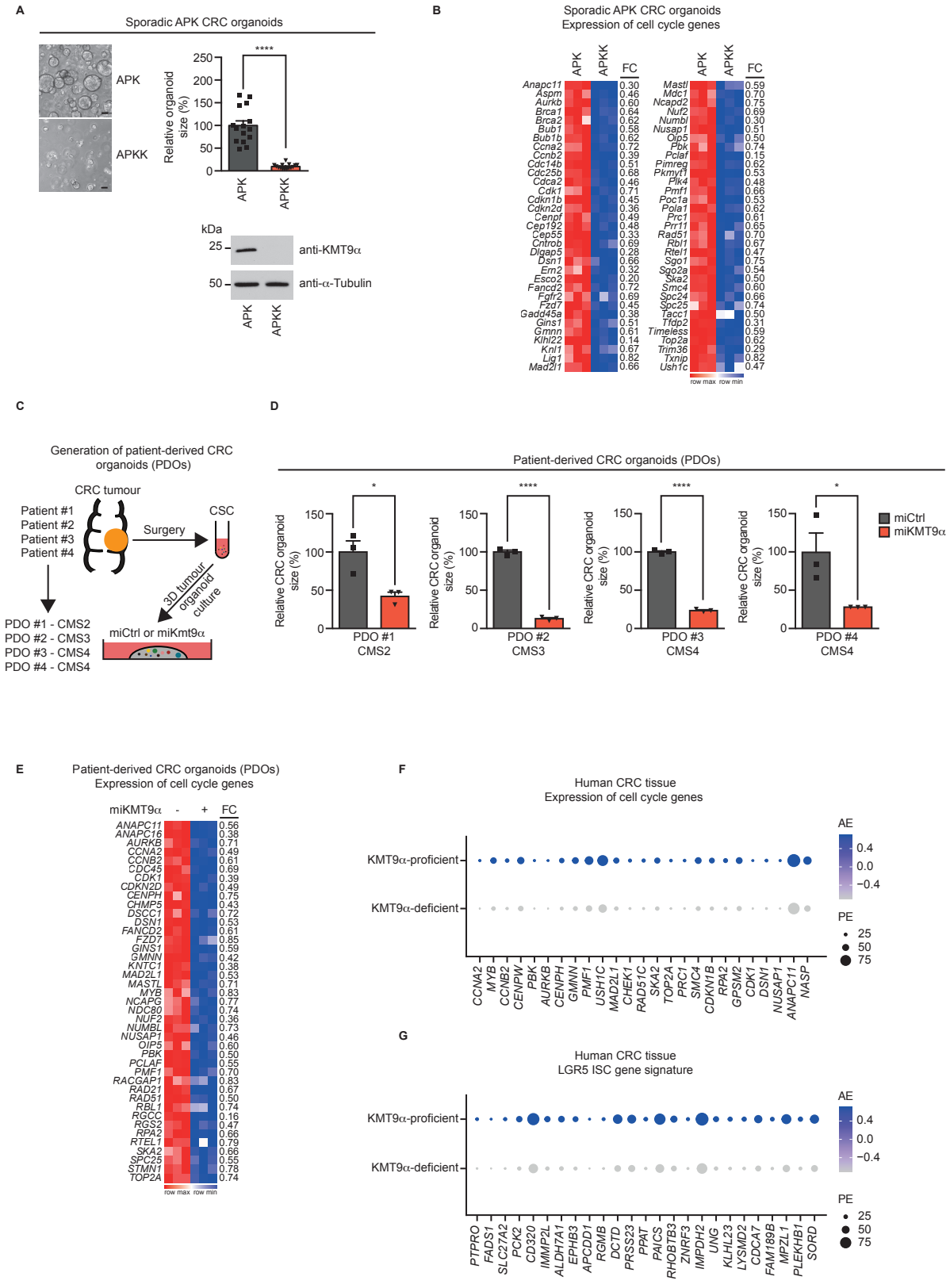

AACR American Association for Cancer Research

Cancer Research

The Journal of Cancer Research (1916–1930) | The American Journal of Cancer (1931–1940)

KMT9 controls stemness and growth of colorectal cancer

Christopher Berlin, Felicie Cottard, Dominica Willmann, et al.

Cancer Res Published OnlineFirst November 4, 2021.